JAAS FULL PAPER
www.rsc.org/jaas

Evaluation of photometric errors in absorption measurements using spatially resolved continuum source graphite furnace atomic absorption spectrometry

James Harnly,[a] Albert Gilmutdinov,[b] Marcus Schuetz[a] and James Murphy[a]

[a]*US Department of Agriculture, Agricultural Research Service, Beltsville Human Nutrition Research Center, Food Composition Laboratory, Building 161, BARC-East, Beltsville, MD 20817, USA*
[b]*Department of Physics, Kazan State University, 18 Kremlevskaja St., Kazan 420 008, Russia*

Received 31st May 2001, Accepted 20th August 2001
First published as an Advance Article on the web 18th October 2001

A continuum source atomic absorption spectrometry (CS-AAS) instrument consisting of a high-resolution echelle spectrometer and a two dimensional charge coupled device (2D-CCD) with a high frame rate was used to measure intensities as a function of height and time in the graphite furnace. The image of the furnace was reduced to a height less than that of the entrance slit to allow the full vertical profile of the furnace to be viewed. Spatially resolved absorbance, A_{SR}, was computed as the average of the computed absorbances for each of the vertical elements, or pixels. Spatially integrated absorbance, A_{SI}, was computed by summing the intensities for each of the vertical pixels and computing a single absorbance. A_{SR} and A_{SI} were computed for three viewing regions: the full image of the furnace (a 6 mm region), the image of the region above the platform (a 4 mm region) and a 2 mm region anywhere within the furnace, which corresponds to a sub-sample of the furnace image with a 2 mm slit height. Photometric errors induced by analyte non-homogeneity were greatest for platform atomization when the full furnace image was viewed and for either platform or wall atomization when a 2 mm sub-section of the furnace was viewed. These photometric errors had the potential for producing analytical errors only when a 2 mm sub-section was viewed. Analytical errors introduced by photometric errors for just four elements in a single standard reference material, Citrus Leaves, ranged from +5% to −15%. These results suggest that photometric error is problematic for conventional line source AAS.

Introduction

Photometric accuracy of absorbance measurements is difficult to achieve with electrothermal atomic absorption spectrometry (ETAAS). The transient nature of the analyte signal and the interaction of the analyte with the furnace wall and the sample matrix produce a constantly changing and non-homogeneous spatial distribution of the analyte. This lack of homogeneity means that the spatial distribution of the source intensity, the position of the entrance slit with respect to the image of the furnace and the mode of absorbance calculation can affect the measured absorbance. Gilmutdinov and Harnly[1] have reported that achieving photometric accuracy requires integration in the absorbance domain with respect to wavelength, height in the furnace and time. The spectroscopic community is well aware of the necessity of a small time interval (high data acquisition frequency, usually 60 Hz)[2,3] to ensure the temporal accuracy for the transient furnace signals. The advantages of enhanced spectral and spatial resolution, as advocated by Harnly and co-workers[4,5] and Gilmutdinov and co-workers,[6–11] are less well recognized. Spatial resolution, in particular, deserves further investigation since the strong possibility exists that the photometric errors may vary systematically with the analyte matrix and thus give rise to analytical errors.

True spatial integration requires the measurement of transmitted intensities with respect to width and height in the furnace. This can only be achieved using a notch filter, to isolate the spectral region of interest, and a two-dimensional array detector to collect the spatial data. Gilmutdinov and co-workers[9–11] have used this approach to characterize the spatial distribution of the radiant intensity of several sources and the spatial distribution of analyte atoms and molecular components. Unfortunately, the low spectral resolution provided by the filter and the low frame rate of the two-dimensional CCDs are not well suited for quantitative determinations in a graphite furnace. Use of a medium-resolution spectrometer provides higher spectral resolution (up to 0.03 nm), but necessitates elimination of data for one spatial dimension. With a spectrometer, intensity data can be collected as a function of wavelength and furnace width, or wavelength and furnace height. With the dosing hole at the top of the furnace and the platform at the bottom of the furnace, collection of intensities as a function of height provides more information.

Holcombe and co-workers[12–14] used a rotating mask and a conventional line source AAS (LS-AAS) to divide the transmitted intensities of a small furnace (CRA-90, Varian Associates, Palo Alto, CA, USA; 3 mm id and 9 mm length) into nine vertical sections. They used this instrument to observe absorbance as a function of height in the furnace for Al, Au, Co, Cu, In, Mn and Pb. For every element, they observed an analyte gradient, decreasing concentration with increasing height in the furnace. This gradient was present most strongly during the leading edge of the peak and disappeared at some point during the tail of the peak. Since the focus of Holcombe's papers was on atomization mechanisms, no attempt was made to characterize the photometric error. Holcombe's work suggests that as interaction of the analyte with the graphite surface of the furnace increases, the gradient becomes steeper.[13,14] Thus, the photometric error arising from non-homogeneous distribution of the analyte can be expected to increase as the analyte-wall interactions increase.

Gilmutdinov *et al.*[15] recently used a linear photodiode array (PDA) to examine the vertical cross section of the graphite

DOI: 10.1039/b104784c

furnace (HGA-500, PerkinElmer Instruments) used with LS-AAS. The read rate of the PDA limited the temporal frequency to 31 Hz. They reported photometric and analytical inaccuracies for Cd in standard reference material (SRM) 1572, Citrus Leaves, and Pb in SRM 1573, Tomato Leaves. These errors were attributed to the inhomogeneous distribution of analyte atoms in the furnace and to variations in the inhomogeneity introduced by the sample matrix. Examination of their data for Cd and Pb reveals concentration gradients similar to those observed by Holcombe over almost the entire lifetime of the analyte peaks. The analytical error arose from difference in the gradients for the standards and the samples.

Harnly *et al.*[5] have constructed a new version of a continuum source-atomic absorption spectrometry (CS-AAS) instrument that is capable of high spectral (horizontal axis) and spatial (vertical axis) resolution. This instrument employs a two-dimensional charge coupled device (2D-CCD) and is capable of acquiring 90 frames of data per second. The instrument optics reduce the furnace image by a factor of approximately 7 to produce an image at the exit plane that is 0.85 mm tall. Thus, the vertical profile of the furnace is viewed by 40–45 pixels (depending on the distance between the lens and the spectrometer). This instrument allows integration in the absorbance domain with respect to wavelength, height in the furnace and time.

This study employed the CS-AAS instrument described above to investigate the non-homogeneity of the distribution of Al (309.3 nm), Cr (357.9 nm), Cu (324.7 nm) and Pb (283.3 nm) atoms in the furnace. The effect of the non-homogeneous distribution of the analytes on photometric error was investigated for atomization from the wall and platform for three different regions (the full image of the furnace—a 6 mm region; the image of the region above the platform—a 4 mm region; and a 2 mm region anywhere within the furnace vertical diameter—a sub-sample of the furnace image with a 2 mm entrance slit height). SRM 1572 Citrus Leaves was used to examine the effect of differences in photometric errors between samples and standards on the analytical accuracy.

Experimental

Instrumentation

The experimental setup shown in Fig. 1 is similar to that previously described.[5] It consists of a 300 W xenon arc lamp with an integral parabolic reflector (Cermax LX300UV, ILC Technology, Sunnyvale, CA, USA), a longitudinally heated graphite furnace (PerkinElmer, HGA 500, Norwalk, CT, USA), an auto-sampler (PerkinElmer, AS-72), an echelle polychromator (SpectraSpan V, Spectrametrics Inc., now out of business), a 2D-CCD camera (PixelVision, Beaverton, OR, USA) mounted on *X*-*Y*-*Z*-*Φ*-stage (three dimensions and angle of rotation), a "SpectraVideo" controller (PixelVision, Beaverton, OR, USA) and a 200 MHz Pentium PC computer. The 2D-CCD camera is an 86×80 pixel (height by width), back-illuminated, split-frame transfer device and was characterized in a previous publication.[5] Each pixel is 20 μm by 20 μm. The camera is mounted in the position of the photographic plate holder of the spectrometer.

The optical arrangement for the CS-AAS (Fig. 1) differs from that previously described[5] by the insertion of a lens (L1) and aperture (A1) between the xenon arc lamp (CS) and the furnace (GF) to improve collimation of the probing beam and enhance the transmitted intensity. The original lens, L2, focuses the image of the graphite tube center onto the spectrometer entrance slit. A 7 mm aperture, A2, was placed in front of L2 to reduce the effect of the lens spherical aberration. To produce a reduced image shorter than the height of the entrance slit, L2 was moved closer to the spectrometer ($d1 : d2 \approx 1 : 8$).

Over the course of this study, the factor by which the image was reduced varied from seven to ten. This variation occurred because the lenses were re-aligned periodically when changing wavelength to minimize chromatic aberration, to provide maximum light throughput and to flatten the distribution of the probing beam intensity over the furnace vertical diameter (Fig. 2A). For example, when determining copper absorbance at 324.7 nm, an image reduction of 6.8 was achieved by locating the lens 53.4 cm from the furnace and 7.8 cm from the spectrometer. In this case, the 6 mm diameter of the furnace was reduced to an image approximately 0.88 mm high at the entrance slit. Since the image at the exit plane of the spectrometer is also 0.88 mm high, 43 pixels (based on 0.0205 mm per pixel[5]) were necessary to register the image of the furnace.

Spatial resolution and field depth of the optical system were checked by placing thin wires (0.18 mm diameter) horizontally across both ends of the tube and through its center. Fig. 2A shows that the spatial resolution of the spectrometer is better than 0.1 mm and the field depth is greater than the tube length (all the three wires produce similar images). It is interesting that the imaging abilities of the system can be used to monitor the process of insertion of the autosampler pipette into the furnace. Fig. 2B shows a series of profiles acquired during the insertion of the pipette tip into the furnace with a platform during routine use of the autosampler. The bold trace presents the transmitted intensity profile before the autosampler pipette has entered the furnace. Zero intensity at pixels 9 through 14 corresponds to the position of the platform inside the furnace. The lighter traces track the entry of the pipette (arrow) into the furnace. Zero intensity for pixels 22 through 24 marks the time when the pipette has reached its final position at the platform. Fig. 2B also shows that intensity transmitted from the region under the platform (pixels 2–8) can be used for absorbance measurements from this part of the furnace.

The effective slit height of the echelle spectrometer was increased for this study by removing the slit height mask. The

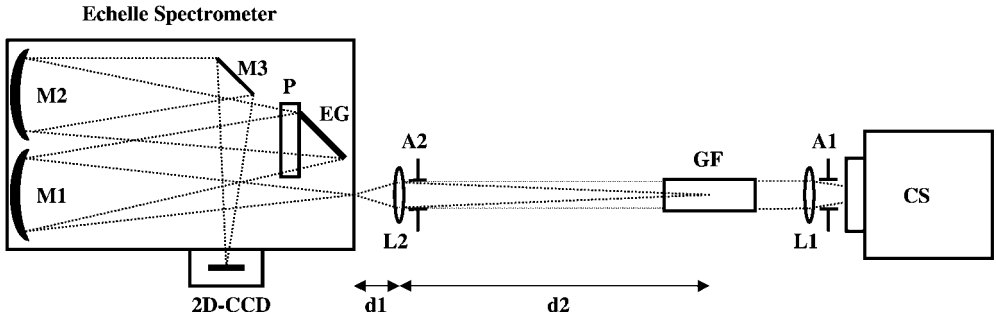

Fig. 1 Block diagram of instrumental set-up: CS, continuum source; L1 and L2, lenses; A1 and A2, apertures; GF, graphite furnace; M1, M2, and M3, mirrors; P, echelle prism; EG, echelle grating; 2D-CCD, two dimensional CCD; d1, distance from lens to entrance slit; d2, distance from furnace center to lens.

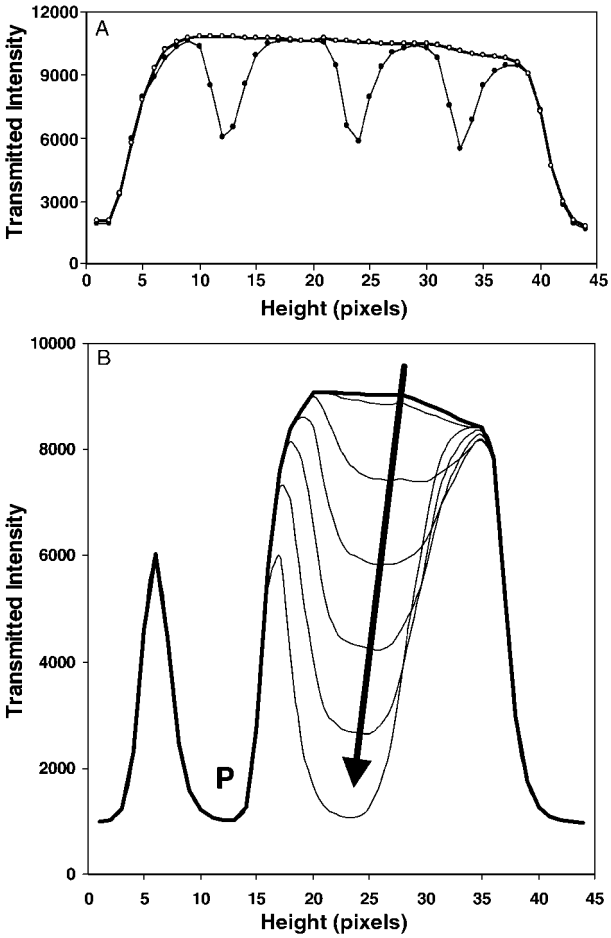

Fig. 2 A, Spatial distribution of transmitted intensity from the primary source over the furnace vertical diameter for empty furnace (○) and for the furnace with three 0.18 mm wires located horizontally at different furnace heights and ends (●). B, Change in the transmitted intensity profile while inserting the autosampler pipette into the furnace: the bold trace shows transmitted intensities through the furnace with a platform, P, before the pipette enters and the lighter traces track the movement of the pipette tip, T, into the furnace.

entrance slit mechanism consists of two orthogonal plates, one with a set of 5 fixed slit width masks and the other with a set of 4 fixed slit height masks. The highest fixed height was 0.5 mm. To permit a larger image to be used, the slit height mask plate was removed and the height of the slit width mask (approximately 1.0 mm) was limiting.

Temperature program

The furnace atomization parameters for Al, Cr, Cu and Pb are shown in Table 1.

Table 1 Operating program for graphite furnace atomizer

			Temperature/°C		
Step	Ramp/s	Hold/s	Wall	Platform	Element
Drying	30	60	120	250	All
Ashing	30	90	300	300	All
Cool down	1	19	20	20	All
Atomization	0	5	2400	2400	Al
			2500	2500	Cr
			2300	2300	Cu
			2000	2000	Pb
Clean out	1	5	2700	2700	All

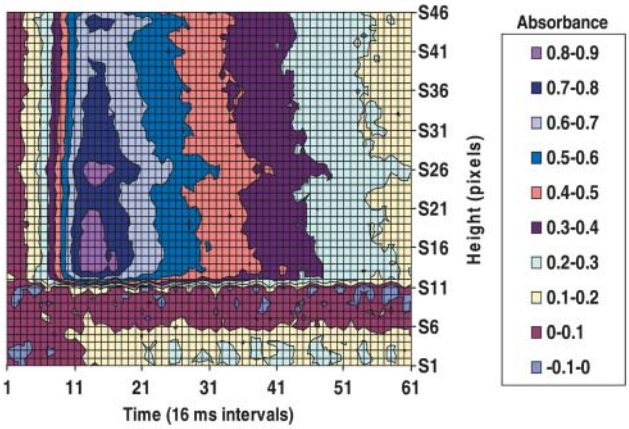

Fig. 3 Contour plot showing absorbance as a function of time and furnace height for the atomization of 150 ng mL^{-1} of Al from a platform.

Data acquisition, storage and processing

Data were acquired at a frame rate of 60 Hz using software written in Labview (National Instruments, Dallas, TX, USA).[5] In this study, all experimental data were acquired for the whole furnace image, *i.e.*, the image of the furnace at the entrance slit was less than the height of the entrance slit.

After acquiring data for the atomization cycle, the raw intensity data (complete frame data for the entire atomization cycle) were recalled and processed using a second Labview program. The processing routine has been described previously.[5] The analyst specifies the height limits (*i.e.*, pixels necessary to cover the height of the image), the wavelength limits (*i.e.*, pixels necessary to cover the absorption profile and sufficient distance to both sides) and the reference frames (acquired prior to the start of atomization) to be used in processing the data. In this study, two sets of height limits were used to process the data for either the full furnace image or for the fraction of the image above the furnace.

For each frame, absorbances were computed for each pixel within the height and wavelength limits using the reference data set. Within a frame, a polynomial equation was fitted to each row of absorbance *versus* wavelength data to remove background absorbance. The absorbance data were then summed over the wavelength interval to produce a linear array of absorbance *versus* height data. In this study, the absorbance *versus* height data were stored for each frame. Thus, an image height of 43 pixels with a 5 s atomization cycle and a 2 s pre-atomization cycle produced an absorbance *versus* height array that was 43 by 420.

Absorbance *versus* height arrays were transferred to Excel (Microsoft Inc., Redmond, WA, USA) for a second processing step. These data could be viewed as a whole using a contour plot (Fig. 3), or absorbance as a function of height could be viewed at any time, or absorbance as a function of time could be viewed at any height (Fig. 4). For each frame, the spatially resolved absorbance (A_{SR}) was determined as the average of the absorbance *versus* height data. Spatially integrated absorbance (A_{SI}), corresponding to absorbance measured by conventional LS-AAS with a single photomultiplier tube, was simulated by converting the absorbance *versus* height array for each frame to an intensity *versus* height array, summing the intensities, and computing a single absorbance. The photometric error was computed in 3 ways:

$$\text{Absolute photometric error} = A_{SR} - A_{SI} \quad (1)$$

$$\text{Percent photometric error} = 100\% \frac{A_{SR} - A_{SI}}{A_{SR}} \quad (2)$$

$$\text{Percent integrated photometric error} = 100\% \frac{\sum_{time} A_{SR} - \sum_{time} A_{SI}}{\sum_{time} A_{SR}} \quad (3)$$

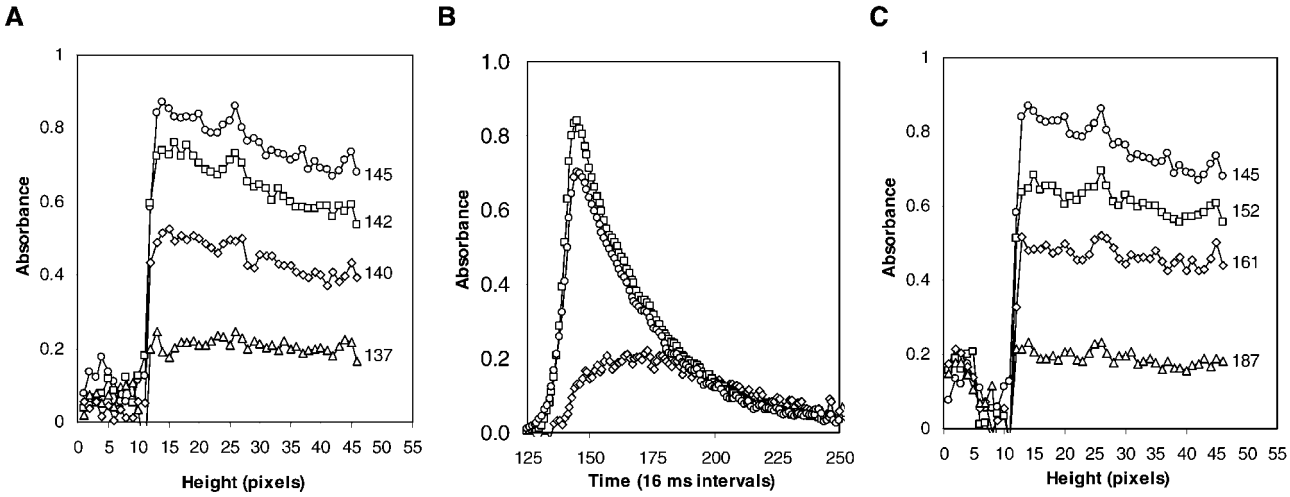

Fig. 4 Platform atomization of 150 ng mL^{-1} of Al: A, absorbance *versus* furnace height at the peak maximum and at three time intervals on the leading edge of the peak; B, absorbance *versus* time (○) just below the top of the furnace, (□) just above the platform, and (◇) below the platform; and C, absorbance *versus* furnace height at the peak maximum and at three time intervals on the trailing edge of the peak. The numbers of the plots in A and C correspond to the time interval in B.

Percentage photometric error was problematic when absorbance was close to zero; division by a small value produced a highly noisy plot. Under these circumstances, the absolute photometric error was more useful. The percentage integrated photometric error provided a better understanding of how the photometric errors influenced the analytical peak areas (absorbance integrated with respect to time).

Simulation of reduced slit height that viewed approximately 1/3 of the full furnace image (*i.e.*, viewed 2 mm of the 6 mm image) was achieved mathematically using the Excel spreadsheet. If the furnace image was 45 pixels, then a 15 pixel high window was used. The position of the window was characterized by the position of the center of the slit. Thus, for a 45 pixel image of the furnace, the lowest and highest possible positions of the center of the slit are pixels 8 and 38. The slit was then moved in 1 pixel increments between these two extremes. This approach was used for the model and the experimental data.

Standards and sample preparation

The SRM 1572 Citrus Leaves sample was prepared by digesting approximately 0.5 g of material in 50% nitric acid. Drops of 10% H_2O_2 were added as necessary to complete the digestion. The solution was then diluted to 10 mL. Appropriate dilutions of the sample solution were made to provide 150 ng mL^{-1}, 120 ng mL^{-1}, 27 ng mL^{-1} and 50 ng mL^{-1} solutions of Al, Cr, Cu and Pb, respectively. Standards of equal concentration were prepared for Al, Cr, Cu and Pb by appropriate dilution of 1000 μg ml^{-1} stock solutions. Sample sizes of 10 μL were deposited in the furnace using the autosampler.

Results and discussion

Signal-to-noise ratio

The signal-to-noise ratios (S/N) for all the elements determined in this study were, in general, worse than those previously reported for the 2D-CCD.[5] This poorer performance was the result of the non-optimum arrangement of the optics that reduced the transmitted intensity by a factor of 3 or 4. As shown in Fig. 1, shifting lens L2 closer to the spectrometer to reduce the image of the furnace resulted in a mismatch of the solid angles for L2 and the spectrometer. Consequently, the spectrometer under-sampled the radiation passing through the

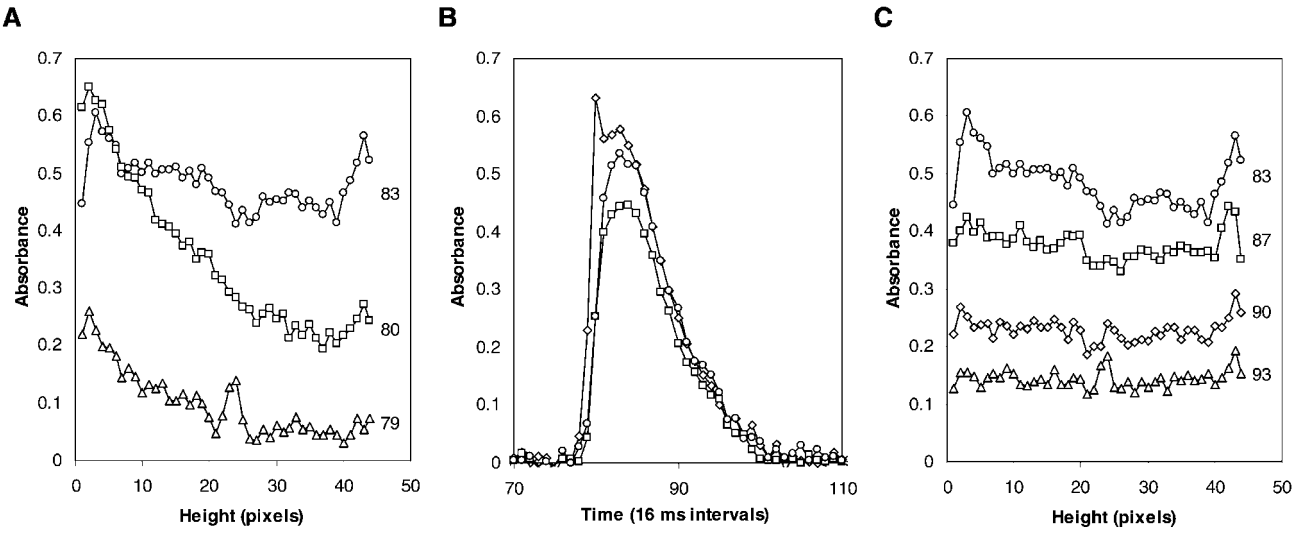

Fig. 5 Wall atomization of 150 ng mL^{-1} of Al: A, absorbance *versus* furnace height at the peak maximum and at two time intervals on the leading edge of the peak; B, absorbance *versus* time (○) just below the top of the furnace, (□) in the middle of the furnace, and (◇) just above the bottom of the furnace; and C, absorbance *versus* furnace height at the peak maximum and at three time intervals on the trailing edge of the peak. The numbers of the plots in A and C correspond to the time interval in B.

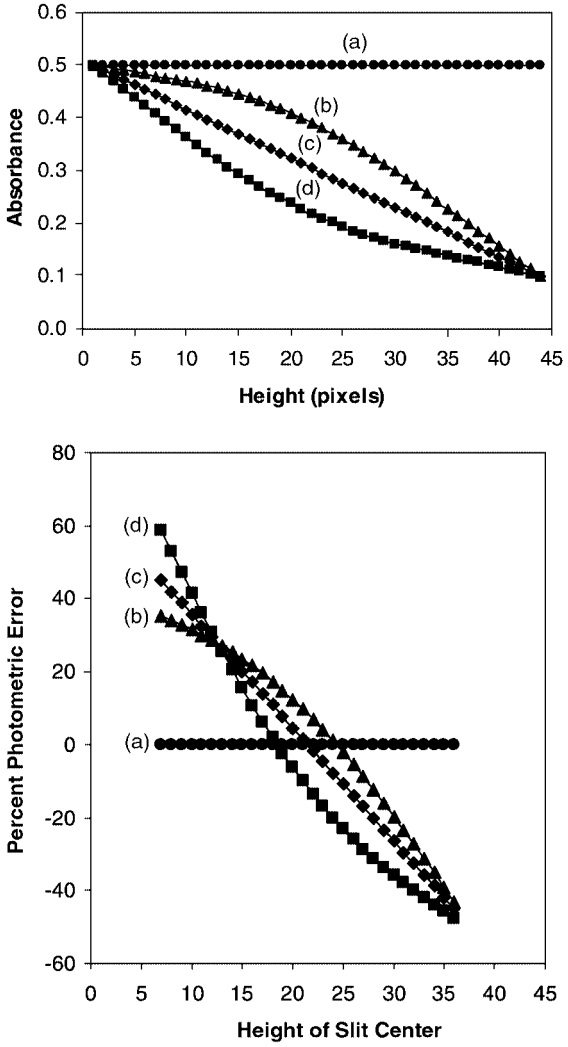

Fig. 6 Model data showing: upper part, the different patterns of absorbance as a function of height in the furnace; and lower part, the resultant photometric error as a function of the center of the slit height. For the upper part, the spatially integrated absorbances measured over the full furnace image were consistently lower than the spatially resolved absorbances by (a) 0.0%, (b) 5.2%, (c) 5.3%, and (d) 6.2%. In the lower part, a 2 mm entrance slit height (15 pixels or 1/3 the furnace height) was systematically scanned from the bottom to the top of the furnace. Absorbance was determined relative to the spatially resolved absorbance, A_{SR}, for the image of the full furnace (all 45 pixels).

entrance slit. Since the instrument is shot noise limited, the reduction in intensity resulted in a reduction of the S/N by a factor of approximately 2. By matching the solid angles for L1, L2 and the spectrometer, the lost intensity could successfully be recovered. Unfortunately, the necessary lenses were not available for this study. Since the main purpose of this study was to examine absorbance as a function of time and height in the furnace, studies proceeded with the poorer S/N.

The plots of absorbance *versus* furnace height suggest a decrease in the S/N far greater than by a factor of 2. It must be remembered, however, that the transmitted intensity has been distributed vertically over 40–45 separate rows of pixels, depending on the exact optical arrangement (see Experimental section). Consequently, the transmitted intensity detected by each row of pixels is reduced by a factor of 40–45 and the S/N will be reduced by approximately a factor of 6.5. Vertical binning of the array pixels was not used for any of the determinations in this study. In the case of Pb, a 3-point sliding average smoothing was applied vertically to improve the S/N. In all other cases, the absorbance data were not smoothed and represent the data collected for each pixel.

Absorbance *versus* height in the furnace

Aluminum. The contour plot in Fig. 3 shows a 46×61 (height *versus* time) absorbance data sub-array of the 46×420 data array generated by 5 s platform atomization of 150 ng mL^{-1} of Al. The 46 pixel height of the image indicated that the image of the furnace on the entrance slit of the spectrometer was 0.94 mm high, a reduction factor of 6.4. On the vertical axis, S1 corresponds to the pixel viewing transmitted intensity at the lowest point in the furnace and S46 corresponds to the pixel viewing transmitted intensity at the highest point in the furnace. The platform, a region for which there was no transmitted intensity and therefore no absorbance, provided a horizontal band of zero absorbance for pixels S6-S11. Deviation from homogeneous absorbance above the platform is demonstrated by the non-vertical iso-absorbance lines.

Fig. 4 provides alternative views of the atomization cycle. Fig. 4B shows absorbance *versus* time just below the top of the furnace, just above the platform and below the platform (see Fig. 4 legend). It can be seen that absorbance was consistently lower below the platform (than above it) until approximately 1 s after the appearance time (at time 185 in Fig. 4B). The analyte absorbance was consistently higher just above the platform than at the top of the furnace. This can be seen more clearly in Fig. 4A and C, where absorbance is plotted as a function of height for the peak maximum and for three time intervals on the leading and trailing edges of the peak, respectively. The plot for the peak maximum is common to both Fig. A and C as a reference. An absorbance gradient (decreasing absorbance *versus* height) can be seen over most of the peak. The gradient was greatest during the leading edge.

Fig. 5 shows plots analogous to Fig. 4 for the atomization of 150 ng mL^{-1} of Al from the furnace wall. Fig. 5A and C shows absorbance maxima close to both walls providing a concave shape superimposed on a decreasing absorbance *versus* height gradient. In Fig. 5B, absorbance measured near the top, near the bottom and in the middle of the furnace are plotted *versus* time. These plots clearly show absorbance near the walls was always greater than at the furnace center. This pattern of Al atom distribution was previously noted by Gilmutdinov.[9] He attributed this effect to the more reducing conditions (greater C : O ratio) and the higher gas temperatures near the walls that decreased the formation of Al_2O_3 and enhanced the atomic Al concentration. For platform atomization, the introduction of Al into a hotter, more uniformly heated gas phase minimized this effect. Although there was still a hint of a maximum near the top of the furnace, it was not nearly as obvious as that observed for atomization from the wall.

Copper. The absorbance *versus* time and absorbance *versus* height plots for the atomization of 80 ng mL^{-1} of Cu from the platform and 27 ng mL^{-1} of Cu from the wall were very similar to those for Al (Figs. 4 and 5) and hence are not shown. Like Al, the steepness of the absorbance *versus* height gradient during the leading edge of the signal is much greater for wall atomization. For both modes of atomization, the gradient was undetectable during the trailing edge of the peak. In addition, the gradient had a convex shape during the peak maximum and during the trailing edge. This suggests a slightly lower analyte concentration near the platform and the top of the furnace. This may be the result of adsorption of the Cu atoms on the graphite surface. Like Al, the Cu atom concentration below the platform generally lagged behind the concentration above the furnace until late in the atomization cycle.

Holcombe and co-workers[12–14] hypothesized that the decreasing absorbance *versus* height gradient observed for Cu during the leading edge of the signal was the result of the continuous adsorption–desorption interaction of atoms with the graphite surface. Since the source of atoms is the bottom of the furnace, a decreasing gradient (from bottom to top) is

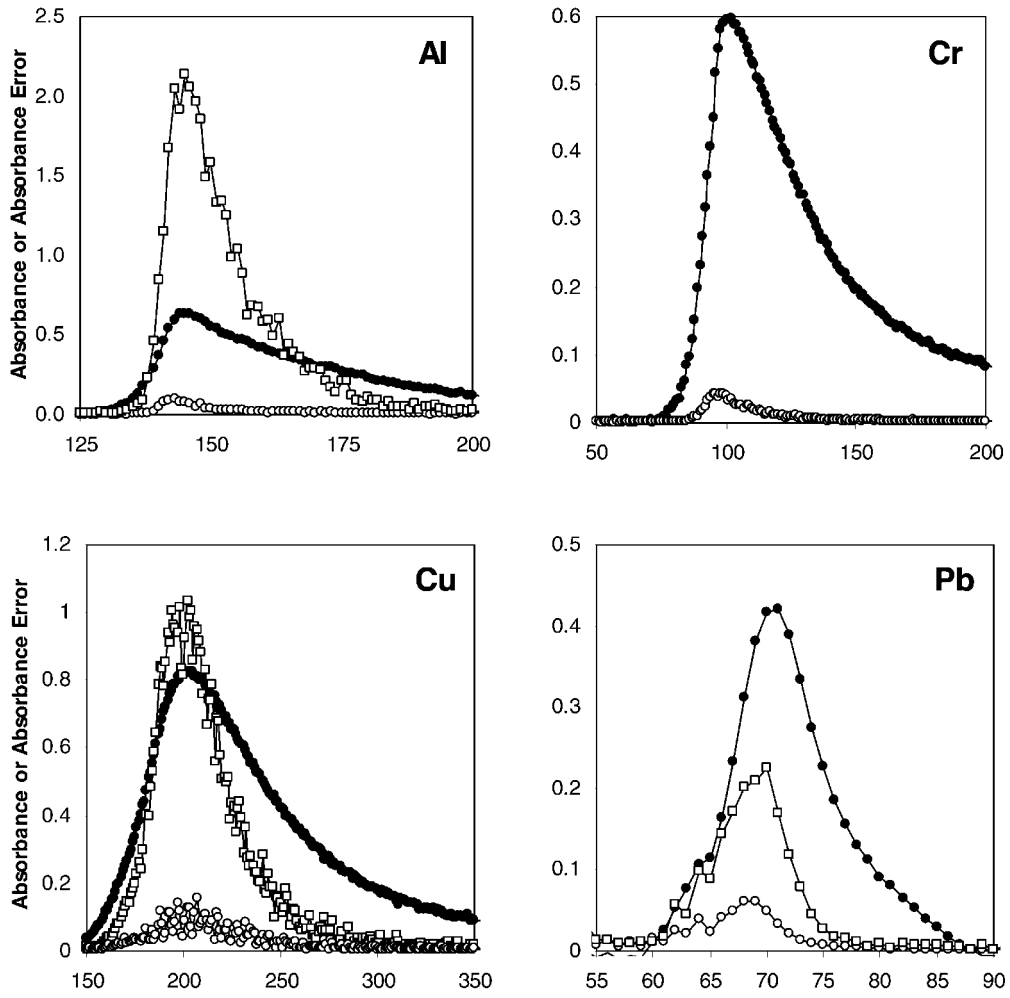

Fig. 7 Experimentally determined absorbance and photometric error as a function of time for Al, Cr, Cu and Pb atomized from a platform: (●) spatially resolved absorbance, A_{SR}, for the full furnace image; (□) absorbance error ($A_{SR}-A_{SI}$) multiplied by a factor of 10 obtained for the full furnace image; and (○) absorbance error multiplied by a factor of 10 obtained for the full image of the furnace above the platform.

observed until uniform coverage of the entire furnace surface is achieved. Working against uniform coverage is the loss of atoms from the dosing hole and the ends of the tube. Thus, each atomization is a race to see if uniform surface coverage can occur before the bulk of the analyte is lost from the furnace.

In Holcombe's work, a drop in absorbance of 0.1 between the bottom and top of the furnace was observed for Co, Cu, Mn and Pd. This was interpreted as evidence for a moderately strong adsorption of these elements on the graphite surface. The gradient was significantly less for Au and In, suggesting that relatively elastic collisions take place with the furnace wall. For Co, Cu, Mn and Pd, the gradient persisted from the appearance of the signal until half way through the tail of the peak. For Au and In, the gradient disappeared shortly after the peak maximum. The gradient for Al was steeper than that observed for any of the other elements and persisted throughout the peak. It is difficult to draw any conclusions about the interaction of Al with the graphite since there is still considerable debate concerning the role of Al oxides and carbides in the formation of Al atoms.

Chromium. The absorbance *versus* time and absorbance *versus* height plots for the atomization of 120 ng mL^{-1} of Cr from the platform and the wall were also similar to those for Al (Figs. 4 and 5). Atomized from the wall, the leading edge of the Cr peak exhibits a slightly convex shape superimposed on a linear gradient. The gradient disappeared during the trailing edge, but the convex shape remained. Almost identical behavior was observed for atomization of Cr from a platform. The data showed that the gradient was slightly worse for platform atomization than wall atomization.

Lead. The absorbance *versus* time and absorbance *versus* height plots for the atomization of 50 ng mL^{-1} of Pb from the platform and the wall were similar to those for Al (Figs. 4 and 5). A concave shape is superimposed on a gradient that decreases with height. Maxima can be seen near the top and bottom of the furnace during the leading edge for atomization from the wall. The maxima were not visible on the trailing edge, but the S/N was poor. Maxima are also visible for the leading and trailing edges for atomization from the platform. These data suggest that Pb, like Al, tends to form an oxide near the cooler, center of the furnace. Like Al and Cu, the atom concentration below the platform does not approach that above the platform until late in the atomization cycle.

Photometric errors

Theoretical considerations. Modeled data were used to examine the photometric error introduced by the non-homogeneous distribution of the analyte, by the non-homogeneous distribution of the source, and by the position of the entrance slit with respect to the image of the furnace (*i.e.*, the sampling interval). It was assumed that the average absorbance obtained with high spatial resolution, A_{SR}, was the best

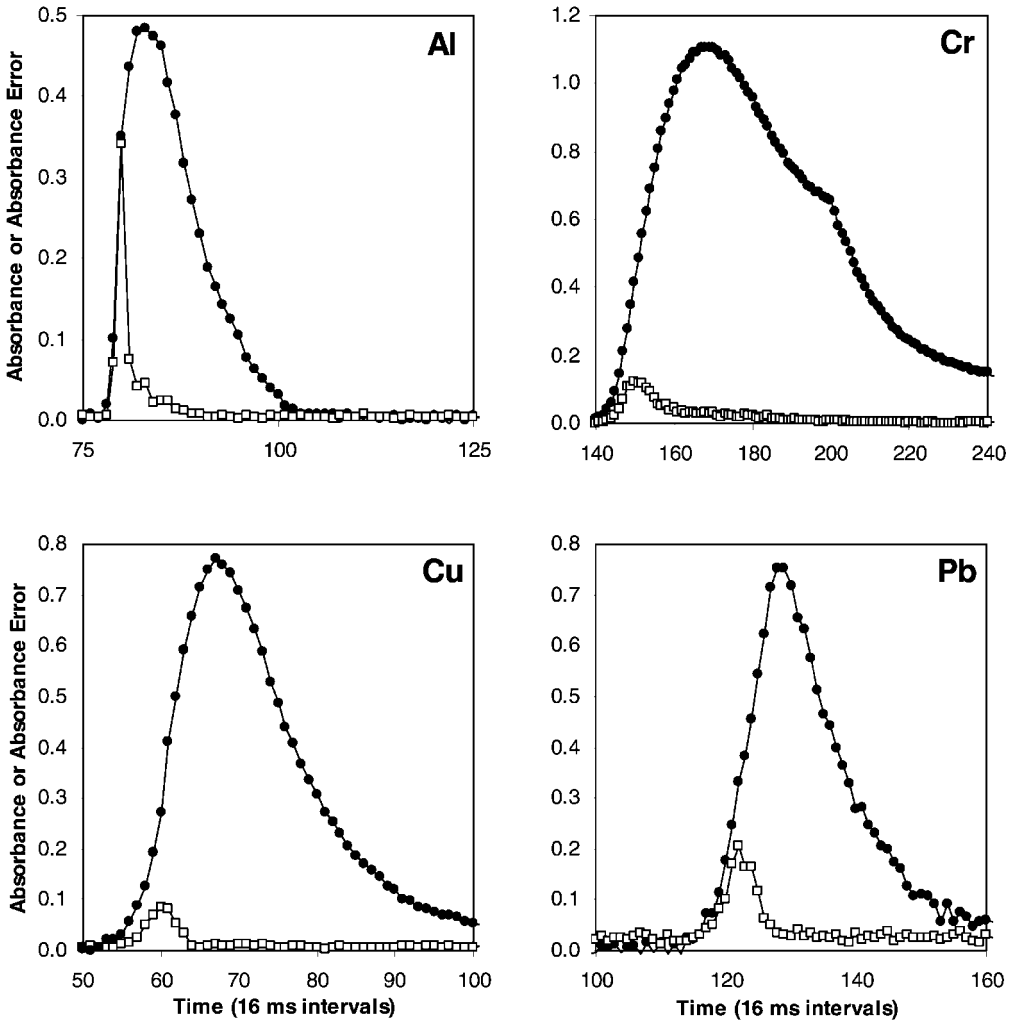

Fig. 8 Experimentally determined absorbance and photometric error as a function of time for Al, Cr, Cu and Pb atomized from the wall: (●) spatially resolved absorbance, A_{SR}, for the full furnace image; (□) absorbance error ($A_{SR}-A_{SI}$) error multiplied by a factor of 10 for the image of the full furnace.

approximation of the "true" analyte absorbance. Photometric error was evaluated as the difference between A_{SR} and spatially integrated absorbance, A_{SI}, as shown in eqns. (1)–(3). If the analyte was homogeneously distributed in the furnace, the mode of calculation (A_{SR} *versus* A_{SI}), the source homogeneity and the sampling interval did not affect the analytical absorbance. If the analyte is distributed in a non-homogeneous manner, each of these factors can introduce photometric errors. If the sample matrix affects the analyte distribution, each of these factors can also result in analytical errors.

Plots of homogeneous (plot A) and different types of non-homogeneous (plots B and C) analyte absorbance are shown in Fig. 6 (upper) as a function of height in the furnace. All four plots correspond to patterns observed for the experimental data reported in the previous section. The model assumed that the furnace image had been reduced by a factor of 6.8 (a value similar to the instrumental arrangement), *i.e.*, the 6 mm vertical cross section of the furnace is observed by 44 pixels. Two viewing modes were considered: the first viewed the entire vertical image of the furnace (6 mm or 44 pixels) and the second viewed 1/3 of the image (2 mm or 15 pixels). The latter mode was intended to imitate conventional LS-AAS that frequently uses a 2 mm slit height to avoid emission from the furnace walls. The 2 mm slit height samples a sub-section of the intensities transmitted through the furnace. The sampled sub-section is variable between experiments, but is constant within an experiment. As described in the Experimental section, the spatially resolved absorbance, A_{SR}, was computed as the average absorbance of the viewed pixels. The spatially integrated absorbance, A_{SI}, was computed by converting the absorbances of the viewed pixels to transmitted intensities, summing the intensities and computing a single absorbance. The percentage photometric error was computed as described in eqn. (2).

If the full image was viewed, A_{SR} values for each of the four plots (a–d in Fig. 6 (upper)) were 0.500, 0.352, 0.300 and 0.248, respectively. Corresponding A_{SI} values for the full image were 0.500, 0.334, 0.284 and 0.232 (0.0%, 5.2%, 5.3% and 6.2% lower). Plot a (0% error) illustrates the fact that the method of computation (A_{SR} *versus* A_{SI}) was not important if the analyte concentration was homogeneous. Superimposing a concave or convex shape (plots b and d) on top of a linearly decreasing (plot c) gradient makes little difference in the error.

The linearly decreasing gradient (plot c) was evaluated further. Table 2 presents a summary of results obtained with systematic variation of the minimum absorbance and change in absorbance (difference between the maximum and minimum). In general, the error was the greatest when the minimum absorbance was lowest and change in absorbance was greatest (9.5% with a minimum absorbance of 0.01 and a change in absorbance of 0.5). More extreme minima and changes in absorbances could have been used, but the values presented in Table 2 provide a reasonable representation of the experimental values observed in the previous section.

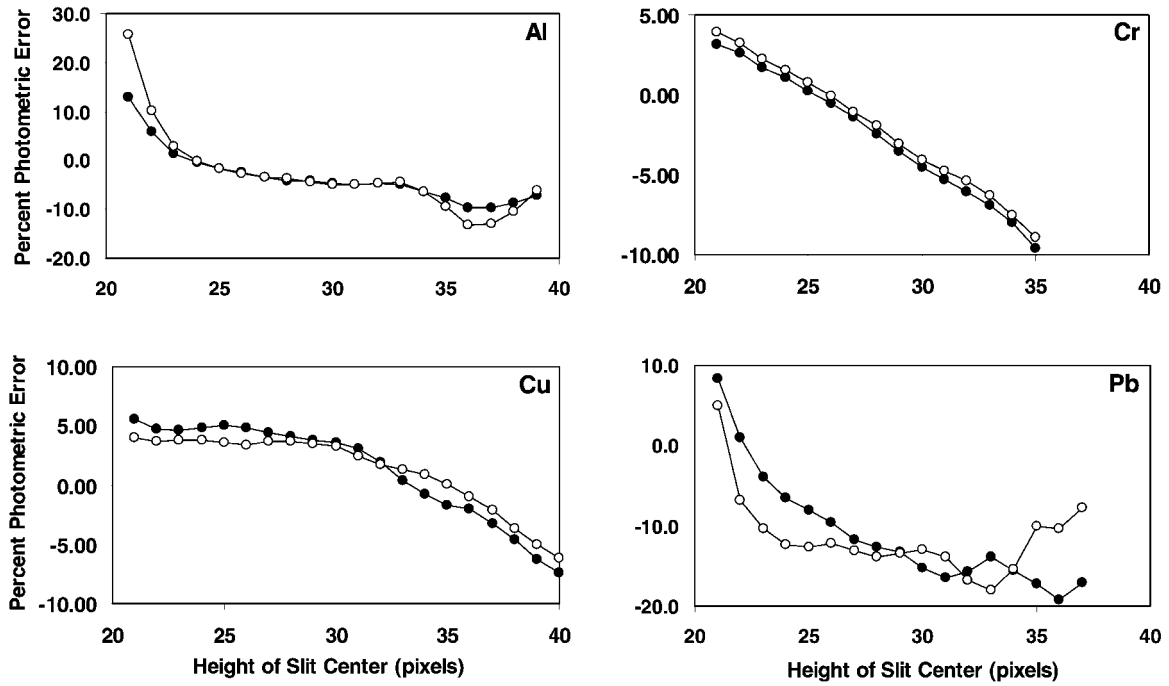

Fig. 9 Experimentally determined photometric error for Al, Cr, Cu and Pb standards (●) and samples (○) as a function of the height of the center of a 2 mm entrance slit height for platform atomization. Percentage error was determined relative to the spatially resolved absorbance, A_{SR}, computed for the full image of the furnace above the platform. Results are analogous to those presented for the model data in Fig. 12.

Table 3 presents results for analyte absorbances identical to those modeled in Table 2, except that a systematic change in the source intensity (from 100% to 32% transmission) has been added. The change in source intensity corresponds to a change in background absorbance from 0.01 to 0.5. With both the analyte and background absorbance decreasing linearly, the photometric error increased for all settings, as can be seen by comparing Table 3 with Table 2. Reversal of the background gradient (*i.e.*, analyte absorbance decreasing and background absorbance increasing) reduced the photometric errors at all settings.

Viewing a sub-section of the image of the furnace can further increase the photometric error. In Fig. 6 (lower), the photometric error for a 15 pixel high slit (2 mm) is presented as a function of the position of the slit center. The photometric error was computed as described in eqn. (2) except that A_{SI} was computed using 15 pixels and A_{SR} was computed using all 44 pixels. Thus, the plots in Fig. 6 (lower) reflect errors arising

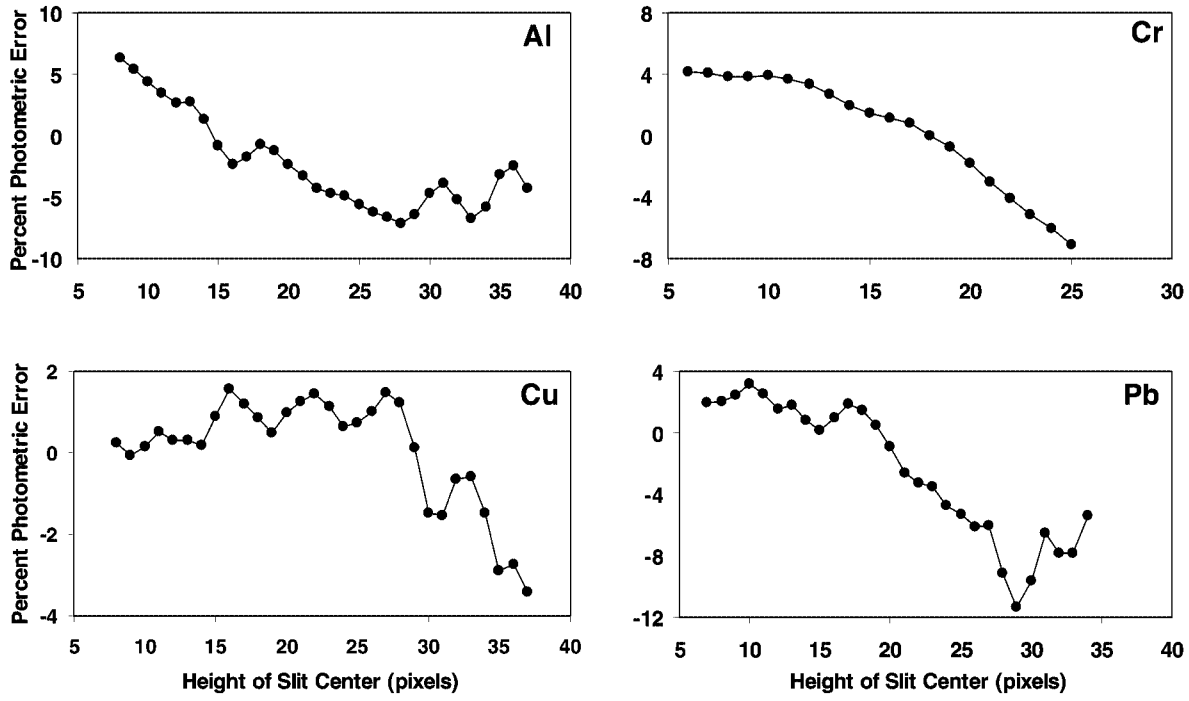

Fig. 10 Experimentally determined photometric error for Al, Cr, Cu and Pb standards as a function of the height of the center of a 2 mm entrance slit height for atomization from the furnace wall. Percentage error was determined relative to the spatially resolved absorbance, A_{SR}, computed for the full furnace image. Results are analogous to those presented for the model data in Fig. 6 (lower).

Table 2 Percent photometric error as a function of initial absorbance and change in absorbance obtained with modeled data for viewing of the full furnace image

Initial absorbance	Change in absorbance					
	0.0	0.1	0.2	0.3	0.4	0.5
0.01	0.0	1.7	3.6	5.6	7.6	9.5
0.1	0.0	0.7	2.0	3.6	5.3	7.1
0.2	0.0	0.4	1.3	2.6	4.0	5.5
0.3	0.0	0.3	1.0	2.0	3.2	4.5
0.4	0.0	0.2	0.8	1.6	2.7	3.8

Table 3 Percent photometric error as a function of initial absorbance and change in absorbance in the presence of background absorbance (at each setting, the background absorbance changed linearly with the analyte absorbance, from 0.01 to 0.5) obtained with modeled data for viewing of the full furnace image

Initial absorbance	Change in absorbance					
	0.0	0.1	0.2	0.3	0.4	0.5
0.01	0.0	17.9	21.2	23.5	25.6	27.4
0.1	0.0	7.2	11.7	15.1	17.9	20.4
0.2	0.0	4.3	7.8	10.8	13.4	15.8
0.3	0.0	3.1	5.8	8.4	10.7	13.0
0.4	0.0	2.4	4.7	6.8	8.9	11.0

from non-homogeneous distribution of the analyte and positioning of the entrance slit with respect to the image of the furnace. With a 15 pixel high slit, the lowest and highest positions for the slit center are 8 and 37, respectively. The percentage photometric error ranged from 60% to −55% depending on the slit position and the non-homogeneous absorbance pattern.

Full furnace image. Photometric errors were computed for the experimental data for Al, Cr, Cu and Pb as described in the Experimental section. Figs. 7 and 8 present absolute photometric errors [eqn. (1)] as a function of time for Al, Cu, Cr and Pb, determined with platform and wall atomization, respectively. For platform atomization (Fig. 7), photometric error was computed for the full furnace image and for the image of the full region above the platform (30–35 pixels). For wall atomization (Fig. 8), photometric error for the full image was computed. In both figures, the photometric errors have been multiplied by a factor of 10 for easier viewing.

Fig. 7 shows that, when viewing the full furnace image, the maximum absolute absorbance error was greater than 0.2, 0.1, and 0.02 for Al, Cu and Pb (note that the absorbance error plots in Fig. 7 have been multiplied by 10). These values correspond to photometric errors of 33%, 12%, and 5% (Table 4). The integrated percentage photometric error [eqn. (3)] ranged from 8 to 14% (Table 4). In each case, the maximum error occurred at the time of maximum analyte absorbance not at the time of the greatest analyte gradient. The source of this dominating error is the difference in absorbance levels above and below the platform. At the peak maximum, this difference was greatest. Absorbance for the lower quarter of the furnace (pixels 1–12 in Figs. 3 and 4) was negligible while absorbance for the upper three-quarters of the furnace (segments 14 and higher) was at its maximum. Consequently, the photometric error was greatest at the peak maximum. In the tail of the peak, as the absorbance below the platform increased and the absorbance above the platform decreased, the difference in absorbance decreased as did the photometric error.

The photometric errors obtained for the image of the full region above the platform were approximately an order of magnitude less than those obtained for the whole furnace image (Table 4). In this case, a 4 mm region of approximately 30 pixels was viewed and used to compute both A_{SR} and A_{SI}. Thus, the dichotomies in absorbance introduced by the platform are ignored. With this viewing region, the maximum errors occurred during the leading edge of the analyte peak and corresponded to the times when the absorbance *versus* height gradient was greatest. The maximum errors were approximately 2% for all 4 elements and the integrated errors were all less than 1% (Table 4).

Table 4 Platform atomization—photometric errors

	Element	Photometric error (%)[a]		Integrated photometic error (%)[b]	
		Full furnace image	Full image above platform	Full furnace image	Full image above platform
Standards					
	Al	33.0	1.8	14.0	0.5
	Cr	—	0.8	—	0.5
	Cu	12.0	1.8	6.3	0.8
	Pb	5.4	2.0	7.6	0.2
Samples					
	Al	19.0	1.5	12.0	2.3
	Cr	—	0.9	—	0.6
	Cu	4.1	0.4	2.2	0.7
	Pb	—	0.5	—	0.3

[a]Largest error for single absorbance value. [b]Error for integrated absorbance.

The absolute absorbance errors obtained by viewing the full image of the furnace with wall atomization (Fig. 8) are similar to those obtained viewing the image of the full region above the platform. The maximum photometric errors ranged from 2 to 10% and the integrated errors ranged from 0.5 to 2% (Table 5). The maximum errors always occurred during the leading edge of the peak and corresponded to the greatest value of the absorbance *versus* height gradient. The photometric errors were greater than those obtained viewing the image of the full region above the platform because the gradients were greater. Undoubtedly this is caused by the more rapid heating rate of the wall that gives rise to more severe temperature gradients and gas expansion effects during the release of the analyte, as compared to the platform.

The results presented in the preceding paragraphs show that the physical barrier of the platform is the largest source of analyte non-homogeneity for the furnace. If a single detector is used, necessitating computation of spatially integrated absorbances, then photometric errors of the magnitude of 8% to 15% are to be expected. Fortunately, most commercial instruments do not view the full furnace image. Entrance slit heights for commercial instruments are usually 2 mm or less and provide views of the region of the furnace above the platform to avoid blackbody emission from the wall or the platform. Thus, the photometric error for a commercial instrument using a HCL or EDL source would be equal to or less than that observed in this study when viewing the full region above the platform.

Photometric errors arising from any non-homogeneous

Table 5 Wall atomization—photometric errors[a] for full furnace image

Element	Photometric error (%)[a]	Integrated photometric error (%)[b]
Al	9.7	1.5
Cr	2.4	0.4
Cu	3.0	2.2
Pb	6.2	0.7

[a]Largest error for single absorbance value. [b]Error for integrated absorbance.

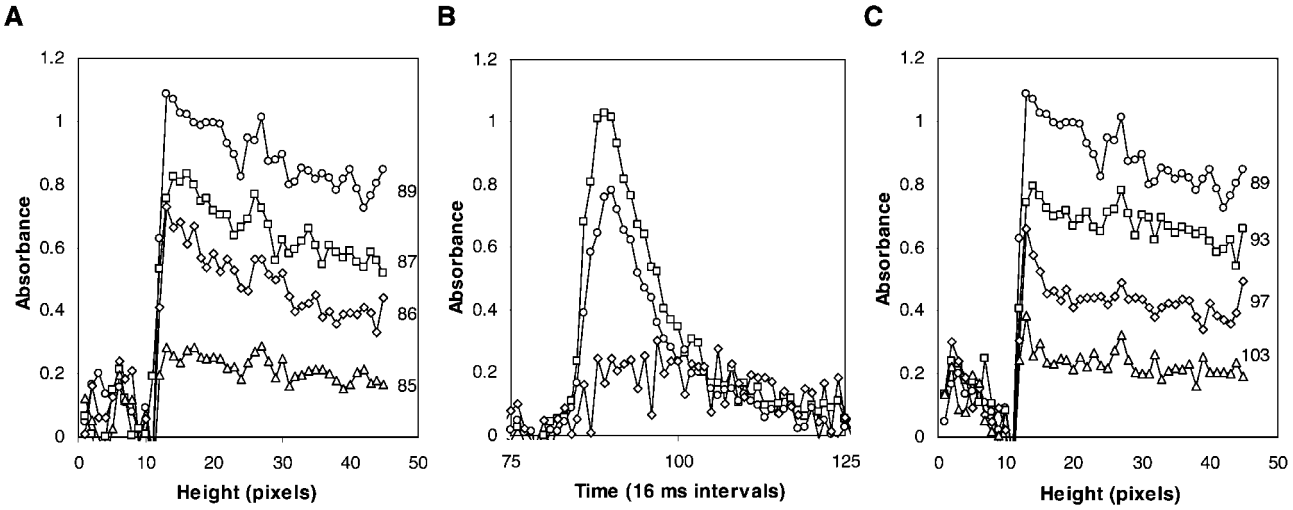

Fig. 11 Atomization of 75 ng mL^{-1} of Al in SRM 1572 Citrus Leaves from a platform: A, absorbance *versus* furnace height at the peak maximum and at at three time intervals on the leading edge of the peak; B, absorbance *versus* time (○) just below the top of the furnace, (□) just above the platform and (◇) below the platform; and C, absorbance *versus* furnace height at the peak maximum and at three time intervals on the trailing edge of the peak. The numbers of the plots in A and C correspond to the time interval in B.

distribution of the source were negligible. First, the distribution of intensities with the current optical alignment was vertically nearly uniform (Fig. 2A and B). Second, no significant background absorption was observed. Consequently, the major sources of photometric errors are the calculation mode and the position of the entrance slit with respect to the furnace.

Effect of a 2 mm high slit. Photometric errors obtained with a 2 mm slit height were obtained by limiting the vertical window for the absorbance calculation, as described in the Experimental section. To appreciate the difference imposed by viewing a sub-section of the furnace, A_{SI} was based on the 15 pixels observed by the slit and A_{SR} was computed for the image of the region above the platform (platform atomization) or for the full image of the furnace (wall atomization). Percentage integrated photometric errors, for atomization from the platform and the wall, are shown in Figs. 9 and 10, respectively, for Al, Cr, Cu and Pb standards. Since the size of the image of the furnace varied with each experiment, the pixel equivalent of a 2 mm slit also varied. Consequently, the maximum and minimum positions of the pixels varied for all the elements in both figures. The photometric errors in Figs. 9 and 10 reflect absorbance differences arising from the calculation mode and from positioning of the slit.

Fig. 9 shows that the range of integrated errors for Al, Cr, Cu and Pb atomized from the platform was 22%, 13%, 13% and 28%. For wall atomization, the integrated error range was 15%, 12%, 5% and 15%. As mentioned in the previous section, A_{SI}, computed for a 2 mm slit height, is an approximation of the performance of conventional LS-AAS. With a continuum source, the full image of the furnace can be viewed, eliminating the error arising from the slit position. This is possible because the intensity of the continuum source is much greater than that of the emission from the furnace walls. This is not possible with commercial LS-AAS instruments because the HCL is less intense. A smaller slit height is necessary to sample only the transmitted radiation passing between the platform and the wall. Thus, greater photometric errors are possible with LS-AAS instruments as illustrated by Figs. 9 and 10.

Analytical error

Analytical errors can arise from photometric errors if the samples and standards produce different patterns of error as a function of height in the furnace. Within an experiment, the spectrometer will consistently view the same physical region in the furnace. If the samples and standards exhibit the same absorbance gradients within this region, there will be no analytical error. If, however, the sample matrix shifts the absorbance gradient, analytical errors will occur.

The only data presented to this point have been for standards. This is because there were no significant differences in the photometric errors observed for the standards and the sample (SRM 1572, Citrus Leaves). This is shown clearly by a comparison of Fig. 11, platform atomization of Al in SRM 1572, with Fig. 4, platform atomization of Al in a dilute acid standard. Such a direct comparison is valid since both standard and sample (based on the certified values) were diluted to produce equally concentrated solutions (see Experimental section). The peak heights were roughly the same (Figs. 4B and 11B), but the appearance times and the widths of the peaks are markedly different. The reduced width undoubtedly gives rise to the poor recovery of the sample (Table 6). The absorbance *versus* height gradients are similar, as is the photometric error as a function of time (Fig. 7 and Fig. 12). Thus, the maximum error and the integrated error for the standard and the sample are in good agreement (Table 4). It is clear that the poor analytical recovery for Al did not come from the photometric error. These poor analytical recoveries undoubtedly arise from the lack of non-optimized atomization parameters and the lack of a matrix modifier.

Table 6 shows that there is no difference in the analytical recoveries for spatially resolved and spatially integrated measurements for all 4 elements when viewing the full furnace image or the image of the region above the platform. The recoveries for Al and Cr were poor (25% and 78%, respectively), but no matrix modifier was used and no attempt was made to optimize the conditions for the analyses. The lack of accurate results is a result of the sample matrix, not

Table 6 Percent analytical recovery for SRM 1572, Citrus Leaves

	Spatially resolved absorbance		Spatially integrated absorbance	
Element	Full furnace image	Full image above platform	Full whole furnace	Full image above platform
Al	29	23	28	23
Cr	—	78	—	78
Cu	99	98	99	98
Pb	—	100	—	100

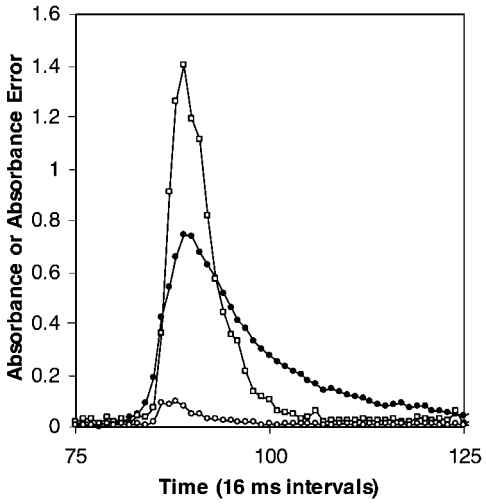

Fig. 12 Experimentally determined absorbance and photometric error as a function of time for the Al data shown in Fig. 11 with atomization from a platform: (●) spatially resolved absorbance, A_{SR}; (□) photometric error multiplied by a factor of 10 obtained viewing the full furnace image; and (○) photometric error multiplied by a factor of 10 obtained for the full image of the furnace above the platform.

photometric error. Table 4 demonstrates that photometric errors arising from the mode of calculation were relatively minor, but measurable, and affected the standards and sample equally. Inspection of the data for all 4 elements shows that the largest experimentally observed absorbance gradient was approximately 0.4. Table 2 shows that, depending on the minimum value, this absorbance gradient should provide errors of 2.7 to 7.6%. The observed maximum errors in Tables 4 (for viewing of the volume above the platform) and 5 ranged from 0.5 to 9.7%. Thus, the photometric errors were in agreement with predicted errors based solely on the absorbance gradient.

When a 2 mm slit height is used, the experimental photometric errors are significantly larger. This is shown in Fig. 9 for samples and standards atomized from a platform and in Fig. 10 for standards atomized from the furnace wall. Examination of Fig. 9 reveals that only Pb shows a marked difference in the percentage error between standard and sample as a function of viewing height. Fig. 13 shows the sample recoveries as a function of viewing height. The range of recoveries for Al, Cr, Cu and Pb are 3.5, 0.3, 3.5 and 20%. The large range of recoveries for Pb correlates with the differences observed in Fig. 9. It should be noted that the ratios of values in Fig. 9 do not produce the values in Fig. 13 because the samples and standards are ratioed to different values. It can be clearly seen that the analytical recoveries of Pb in SRM 1572 can vary from 105 to 85% depending on the positioning of the exit slit with relation to the image of the furnace.

Conclusion

This study demonstrates that accurate absorbance measurements are best achieved with a vertically segmented detector that permits calculation of spatially resolved absorbances. Although a continuum source was used for this study, this conclusion is equally true for a line source. Photometric errors induced in absorbances, based on spatially integrated intensities, by analyte non-homogeneity are greatest for platform atomization when the whole image is viewed and for either platform or wall atomization when a 2 mm sub-section of the furnace is viewed. These photometric errors had the potential for producing analytical errors only when a 2 mm sub-section was viewed. Analytical errors induced by photometric errors for just 4 elements in a single SRM with platform atomization ranged from +5% to −15%. These initial results indicate that analytical error induced by photometric error can be of considerable significance for conventional line source AAS. Further studies are necessary to fully characterize the full effect of photometric error on analytical accuracy.

Acknowledgements

A.G. is grateful to USDA for providing a research grant for travel to USA. The authors acknowledge the contribution of Ms. Ella Green for preparation of the SRM.

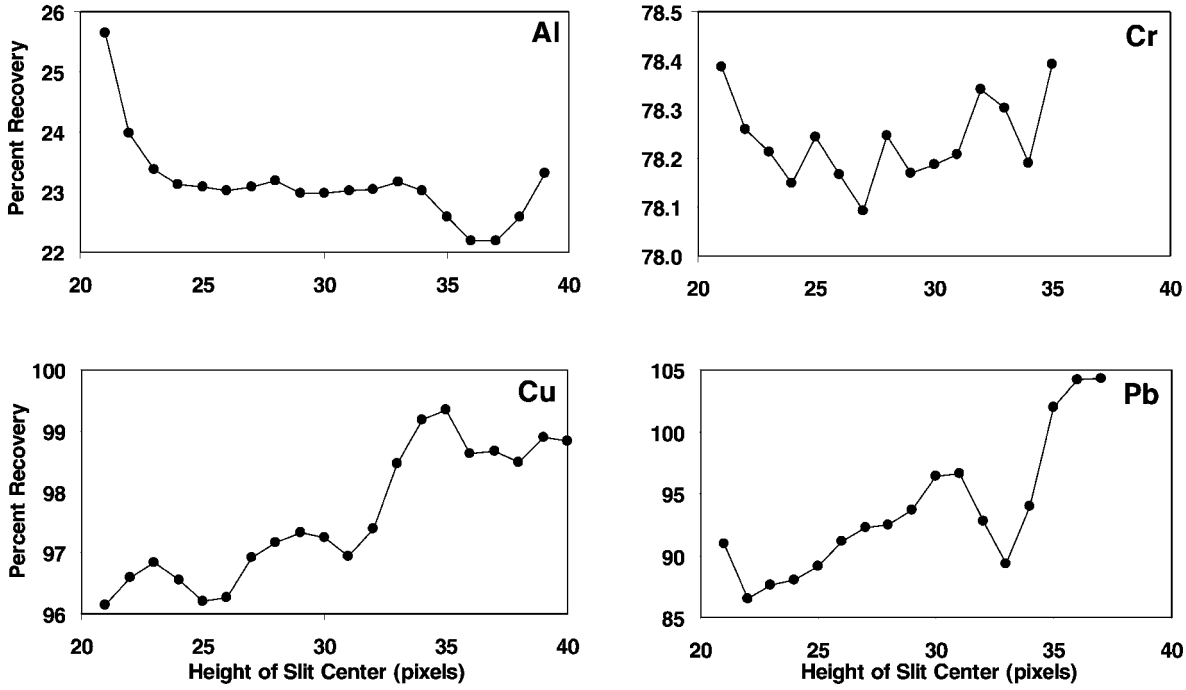

Fig. 13 Analytical recoveries of Al, Cr, Cu and Pb in SRM 1572 Citrus Leaves as a function of the height of the center of a 2 mm entrance slit.

References

1 A. Kh. Gilmutdinov and J. M. Harnly, *Spectrochim. Acta, Part B*, 1998, **53B**, 1003.
2 R. E. Sturgeon and C. L. Chakrabarti, *Prog. Anal. At. Spectrosc.*, 1978, **1**, 5.
3 E. Lundberg and W. Frech, *Anal. Chem.*, 1981, **53**, 1437.
4 J. M. Harnly, C. M. M. Smith and B. Radziuk, *Spectrochim. Acta, Part B*, 1996, **51**, 1055.
5 M. Schuetz, R. E. Fields, J. Murphy and J. M. Harnly, *Spectrochim. Acta, Part B*, 2000, **55B**, 1895.
6 A. Kh. Gilmutdinov, B. Radziuk, M. Sperling, B. Welz and K. Yu. Nagulin, *Appl. Spectrosc.*, 1995, **49**, 413.
7 A. Kh. Gilmutdinov, B. Radziuk, M. Sperling, B. Welz and K. Yu. Nagulin, *Appl. Spectrosc.*, 1996, **50**, 483.
8 A. Kh. Gilmutdinov, B. Radziuk, M. Sperling, B. Welz and K. Yu. Nagulin, *Spectrochim. Acta, Part B*, 1996, **51**, 931.
9 A. Kh. Gilmutdinov, Yu. A. Zakharov, V. P. Ivanov and A. V. Voloshin, *J. Anal. At. Spectrom.*, 1991, **6**, 505.
10 A. Kh. Gilmutdinov, Yu. A. Zakharov, V. P. Ivanov, A. V. Voloshin and K. Dittrich, *J. Anal. At. Spectrom.*, 1992, **7**, 675.
11 A. Kh. Gilmutdinov, Yu. A. Zakharov and A. V. Voloshin, *J. Anal. At. Spectrom.*, 1993, **8**, 387.
12 J. A. Holcombe, G. D. Rayson and N. Akerlind Jr., *Spectrochim. Acta, Part B*, 1982, **37B**, 319.
13 J. McNally and J. A. Holcombe, *Anal. Chem.*, 1987, **59**, 1105.
14 J. McNally and J. A. Holcombe, *Anal. Chem.*, 1991, **63**, 1918.
15 A. Kh. Gilmutdinov, K. Yu. Nagulin and M. Sperling, *J. Anal. At. Spectrom.*, 2000, **15**, 1375.